Turk J Elec Eng & Comp Sci, Vol.19, No.4, 2011, © TÜBİTAK
doi:10.3906/elk-1002-30

Sliding mode controller gain adaptation and chattering reduction techniques for DSP-based PM DC motor drives

Mehmet DAL[1,*], **Remus TEODORESCU**[2]
[1]*Kocaeli University, Electricity and Energy Department of VSK, Kocaeli-TURKEY*
e-mail: mdal@kocaeli.edu.tr
[2]*Aalborg University/Institute of Energy Technology, Aalborg-DENMARK*
e-mail: ret@iet.aau.dk

Received: 11.02.2010

Abstract

In order to achieve and maintain the prospective benefits of sliding mode control (SMC) methodology, the phenomenon known as "chattering", the main obstacle encountered in real-time applications, has to be suppressed. In this study, two promising switching control gain adaptation and chattering reduction techniques are investigated, and the effectiveness of chattering suppression for current regulation of PM DC drives is tested. The sampling rate was also examined to determine how it affects the amplitude of chattering. This paper concentrates on various combinations of observer-based methods in order to find the best solution for chattering reduction. To find a practical solution a tunable low-pass filter (LPF) was used to average the discontinuous control term. The validity of the existing conditions for the gain adaptation methods are examined and observer gain value was determined through simulations. To demonstrate the effectiveness of each method, several experiments were performed on a DSP-based PM DC motor drive system. Then, the newly proposed combinations of these methods were implemented. The hardware implementation results are comparatively presented and discussed.

Key Words: *DC drives, sliding mode control, chattering reduction*

1. Introduction

PM DC motors are still very common in the market due to their cost-effectiveness and robustness. In practice, DC motor drive systems use linear control, as do most industrial applications. These methods, like traditional proportional-integral (PI) control, are simple to design and implement. However, a well-known problem with these methods is that system parameter variations and external disturbances may degrade trajectory tracking. Consequently, designers have tried to improve the performance of closed-loop systems with imperfect knowledge of parameters, either by updating system parameters in the controller during operation or by using robust control

*Corresponding author: Kocaeli University, Electricity and Energy Department of VSK, Kocaeli-TURKEY

methods. Presently, the SMC method is increasingly common as a means to ensure satisfactory performance in the presence of parameter variation and disturbances. Several tutorials pertaining to SMC can be found in [1], [2] and its application to electric drives in [3], [4]. SMC, as a variable-structure-control (VSC) approach, has been widely applied to electric machine drives control, power converters and motion control systems [3]-[8]. The main advantages of SMC are its fast dynamic response, robustness [8], and simplicity in design and implementation [9].

The SMC strategy has 2 kinds of design parameters that should be selected to provide stability and better performance. The first design parameter is the sliding surface parameter by which time-varying [10] or nonlinear [11] sliding surfaces are designed in the literature. However, the control law and stability conditions become more difficult with a complex sliding surface. The second design parameter is the switching control gain of the discontinuous control. In theory, the discontinuous control gain is active in the sliding mode when the system trajectories are on the sliding surface. However, in real-time implementation, chattering occurs, which appears as an undesired oscillation on the system trajectory with finite frequency and amplitude, and leads to low control accuracy, high wear of moving mechanical parts, high heat loss in power circuits, and control loop instability [12]. Two reasons for chattering have been identified [4]: 'unmodeled' dynamics of the system usually disregarded in the control design process, and the inherently limited sample rate in digital controllers. For chattering reduction, several suppression methods have been analysed recently, including switching gain adaptation methods [13], [14], and the observer-based method [15]. Additionally, saturation [16], or use of a shifted sigmoid function [17] instead of a sign function is also used for chattering reduction or elimination. Other chattering suppression methods based on high-order SMC can be found in [18] and the references therein, and information regarding its implementation for DC drives is in [19].

The observer-based method is one of the methods for chattering suppression, but parameter mismatches between the observer and the plant can degrade robustness [20]. The use of an LPF is common and fairly good at capturing the equivalent control from a discontinuous control signal [21].

On the other hand, SMC switching frequency depends on the sampling rate, which causes an undesired effect called discretization chattering [13]. Hence, increasing the sampling rate may decrease the amplitude of the discretization chattering.

The effectiveness of 2 switching gain adaptation methods – 'equivalent-control-dependent' and 'state-dependent' – on chattering suppression has been verified by mathematical analysis and numerical simulation [13], [14]. However, it is reported that these methods were not applicable to systems controlled by an on/off switching mode, which is necessary for electric drives with power electronic converters. Thus, their hardware implementation in a real-life system with the use of a smoothing filter together has been studied in a more recent work [22], and it was observed that the gain adaptation methods and the observer-based method were unsatisfactory when performed separately in conventional SMC. Therefore, in this paper various new combinations of these methods with the observer-based method are studied to find the best solution for chattering elimination. To determine the effectiveness of adaptation methods mentioned above with the use of a smoothing filter as well as an increased sampling rate, several experiments are conducted for current regulation of PM DC motor drives. The chattering reduction methods are each compared experimentally with respect to the observer-based method and new combined methods. The required current estimation is achieved by using a unified sliding mode observer. The averaging operation needed for the equivalent control extraction and for proper current estimation is performed using a tunable LPF.

The results of hardware experiments are comparatively presented and discussed. In addition, system

stability, which must be preserved throughout operation, is tested and recorded. Several simulation tests are performed to determine the proper controller parameters and observer, with regard to system stability.

2. Problem statement

2.1. Dynamic model of a DC machine

Permanent magnet DC machine dynamics can be expressed by the following 2 coupled linear time-invariant (LTI) first-order differential equations:

$$L\frac{di}{dt} = -Ri + u - k_e\omega \tag{1}$$

$$J\frac{d\omega}{dt} = -B\omega + k_t i - t_L \tag{2}$$

where u is the motor supply voltage, i is the rotor current, ω is the angular speed of the rotor shaft, t_L is the load torque, R and L are the resistance and inductance of the rotor winding, respectively, k_e and k_t are the back-emf constant and torque constant of the motor, respectively, J is the total motor and load inertia, and B is the viscous friction coefficient.

As stated in the introduction, traditional model-based linear control can be used due to its simplicity for DC motor drives. However, drive performance is degraded by several motor parameters that are not exactly known and/or vary during operation; therefore, proper tuning and precise knowledge of the motor parameters are necessary to guarantee a desirable performance for current, torque, speed, and position regulations [23]. To achieve this, robust control strategies such as SMC are preferred due to their robustness and faster dynamic response with respect to the traditional linear approaches.

In the field of electric drives, satisfactory current and speed control performance not only depends on control parameterization, but also on accurate current measurement, which is usually performed by hall-effect sensors. These devices contain a current-to-voltage converter, and the temperature of the hall sensor is proportional to the H-bridge converter switching frequency, which has to be limited to keep the switching losses within permitted levels. Consequently, current noises are often significant, and the accuracy of current measurement is degraded [24]. On the other hand, similar to the 3-phase inverter [25], H-bridge converter dynamics can be represented by a first-order system model, which is generally omitted in design consideration.

In light of these matters, a DSP-based DC drive system is used in this study to represent a real-life system, in which the rotor winding acts as a first-order plant for the current control loop, and the dynamics of the hall-effect current sensor and H-bridge converter (as an actuator) together may be considered as 2 cascading first-order systems with a small time constant. This assumption will be taken into account for further consideration on the study of chattering analysis in cases when the discontinuous nature of the H-bridge is not neglected and pulse-width-modulation (PWM) is not used. However, the current ripple caused by inherent discontinuous (on/off) operation of the H-bridge with PWM has an adverse effect on control signal chattering. This may be avoided using an observer-based method, replacing estimated current with measured current in the feedback loop.

2.2. Sliding mode current controller

The design of SMC involves 2 steps: (i), the selection of appropriate switching function s for desired sliding mode dynamics, and (ii), the design of a control for enforcing a sliding motion on selected manifolds in system state space. For current trajectory tracking, the required switching manifold can be described as follows:

$$s = e = i^* - i \tag{3}$$

where e is the current tracking error, i is measured current and i^* is its reference, which can be provided by a speed controller or by a current reference generator. Based on the Lyapunov stability theorem, to enforce a sliding mode on the selected sliding surface s, the desired control must satisfy the existing condition, which can be given by $\dot{V} = s\dot{s} < 0$, since the Lyapunov candidate function is chosen as $V = s^2/2$. This condition must be fulfilled by designed control laws. The first version of the control laws in this paper may be

$$u_1 = M\, sign(s) + u_{FF} \tag{4}$$

where $u_{FF} = k_e\omega$ is a feed-forward term corresponding to the back-*emf* generated on the rotor winding, and M denotes the switching control gain constant. The additional term u_{FF} helps to cancel the term $k_e\omega$ acting in the real system described in (1). For system (1), evaluation of the condition $s\dot{s} < 0$ with help of (4), and replacing the supply voltage u in (3) with the control u_1 results in

$$s\dot{s} = s(\frac{di^*}{dt} + \frac{R}{L}\dot{i}) - \frac{1}{L}M\,|s| \tag{5}$$

which implies the following condition for a sliding mode to exist:

$$|L\dot{i}^* + Ri| < M \tag{6}$$

3. Chattering suppression methods

Chattering mainly occurs due to the non-linearity of the sign function that performs the switching operation and generates a discontinuous control signal. The magnitude of chattering depends on the magnitude of the switching control gain M. In this section, various chattering suppression methods recently presented in [13] and [14] are briefly explained and adapted to current regulation of DC motor drives.

3.1. Averaging operation with LPF

In the implementation of a conventional SMC, the use of an LPF is a popular approximate method to attenuate chattering by extracting the equivalent control u_{eq} from the discontinuous control signal. The equivalent control u_{eq} necessitates the condition $\dot{\sigma} = 0$ for the state trajectory to stay on the switching surface s [3]. Since the implementation is performed by digital controllers, extraction of the equivalent control can be assured by discrete-time filters. A discrete-time first-order LPF structure can be obtained by discretizing its continuous-time version $T_c\dot{u}_{av} + u_{av} = u_n$ using the Euler method as follows.

$$\dot{u}_{av} = \frac{du_{av}}{dt} \cong \frac{u_{av}(k) - u_{av}(k-1)}{T_s} \tag{7a}$$

$$u_{av}(k) = \underbrace{\frac{T_c}{T_c + T_s}}_{a} u_{av}(k-1) + \underbrace{\frac{T_s}{T_c + T_s}}_{1-a} u_n(k) \tag{7b}$$

where T_s is the sampling-time of a digital controller, T_c is the time-constant of the LPF, and $u_{av}(k)$is the average value of the discontinuous control $u_n(k)$ provided by sliding mode controllers at k^{th} sampling intervals. The average value of the discontinuous control is equal to the equivalent control $u_{av}(k) = u_{eq}(k)$ for any preferred control versions used in this study.

To apply (7b), a filter corner frequency f_c $(= 1/T_c)$ must be selected to be smaller than the sampling frequency, f_s $(= 1/\ T_s)$ of the digital controller. To determine the desired corner frequency f_c online, a tunable discrete-time LPF suggested in a recent study [26] is used. This filter structure can be modeled using (7b) as shown in Figure 1, which facilitates adjusting the corner frequencies while the system is operating. Consequently, a rebuild process for code generation is no longer needed at the time of each frequency change. In Figure 1, the SM controller can be altered with any proposed version, and the filter can also be used for the current observer to average the observer discontinuous control signal. In case the purpose of this filter changes, the signal on the sliding surface $s(k)$ must be replaced accordingly.

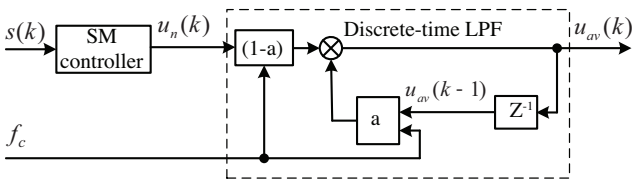

Figure 1. Averaging discontinuous control signal and structure of tunable discrete time first-order LPF with adjustable cut-off frequency.

3.2. State observer-based method

The main purpose of using a state observer in chattering reduction is to exclude unmodeled dynamics from the main control loop [3]. In our case, undesired ripples on the current feedback are created due to the nature of the H-bridge converter on/off operation with PWM. These ripples and disturbances on measured current that are caused by hall-effect devices may reflect as chattering on the control signal. This chattering may be reduced by constructing an auxiliary observer loop with an observer and a new sliding manifold employing the estimated current $\hat{i}$ instead of the measured current i in the feedback loop as shown in Figure 2. In implementation, the current control law (4) or other versions which will be introduced in further sections can be performed without changing the structure, but by only replacing the sliding function with a different function, for example, $\hat{s} = \hat{e} = i^* - \hat{i}$, which is constructed for the observer-based method depending on the estimated current.

For current estimation, a unified sliding mode observer, proposed in [4] for the rotor current and speed estimation, is used. This observer structure is

$$\frac{d\hat{i}}{dt} = -\frac{R}{L}\hat{i} + \frac{1}{L}u - l_1 sign(\hat{s}_i) \tag{8}$$

which is a particular single state example of a non-linear high-gain observer first described by Drakunov [27]. Generally with LTI systems, the goal is to design a high-gain state observer that estimates the state vector

($x = [x_1, x_2, x_3, \ldots x_n]$) using only information from the measurement of output ($y = [1, 0, 0, \ldots 0]x = x_1$), which is a scalar equal to the first state x_1. In our case, statex_1 corresponds to the rotor current i, error $\hat{e}_i = \hat{i} - i$ is the current estimate error, the term $l_1 sign(\hat{s}_i)$ is the nonlinear observer control, l_1 is the observer gain constant that serves a similar purpose as in the typical linear Luenberger observer, and u is the control input, which corresponds to the motor terminal voltage.

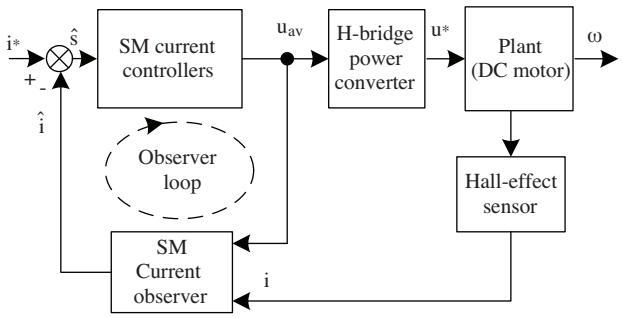

Figure 2. Observer-based sliding mode current control of DC drive system.

In implementation, u is not easy to handle by measurement due to PWM modulated signals at the motor terminal. Thus, it is usually replaced with an average (continuous) value of the control signal (u_1 or others described in later sections) generated by SM controllers. In this case, the voltage drop on the power converter switches and motor brushes are neglected. Therefore, a nonlinear observer control $l_1 sign(\hat{s}_i)$ must be designed in order to enforce the sliding manifold $\hat{s}_i = \hat{i} - i = 0$ by proper selection of observer gain ($l_1 > 0$) and then estimated current $\hat{i}$ can converge to the real current i after a finite time. Moreover, the average value of $l_1 sign(\hat{s}_i)$ is needed for a proper estimation. This can be achieved by passing the term $l_1 sign(s_{\hat{i}})$ through an LPF. For this purpose a tunable filter in Figure 1 can be used. The observer model built with Simulink blocks is shown in Figure 3, which can be used both for simulation and hardware experiments.

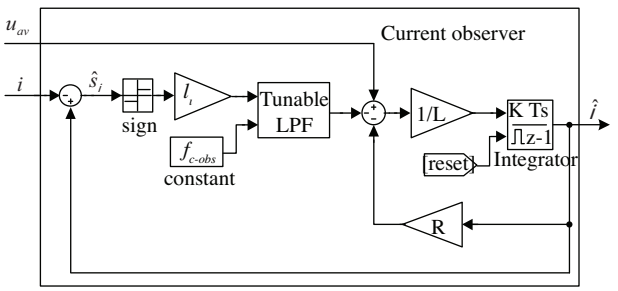

Figure 3. Structure of realized sliding mode current observer.

In general, the effectiveness of an observer is assessed by examining the estimation error dynamic, which can be obtained as follows by subtracting (1) from (8):

$$\frac{d\hat{e}_i}{dt} = -\frac{R}{L}\hat{e}_i + \frac{k_e}{L}\omega - l_1 sign(\hat{e}_i) \tag{9}$$

According to the existing condition $\hat{s}_i \dot{\hat{s}} < 0$, a sliding mode ($\hat{s}_i = \hat{e}_i = 0$) occurs on the observer sliding manifold if the gain l_1 is selected to satisfy the following inequality:

$$|(k_e/L)\omega| < l_1 \tag{10}$$

This leads to the current estimation error $\hat{e}_i$ decaying to zero over time. The gain l_1 should be determined properly to achieve a satisfactory convergence. For this purpose a simulation test was performed and it was observed that the value of gain l_1 must be greater than 8.5, but we selected $l_1 = 20$ in simulation for more satisfaction. This simulation result is shown in Figure 4.

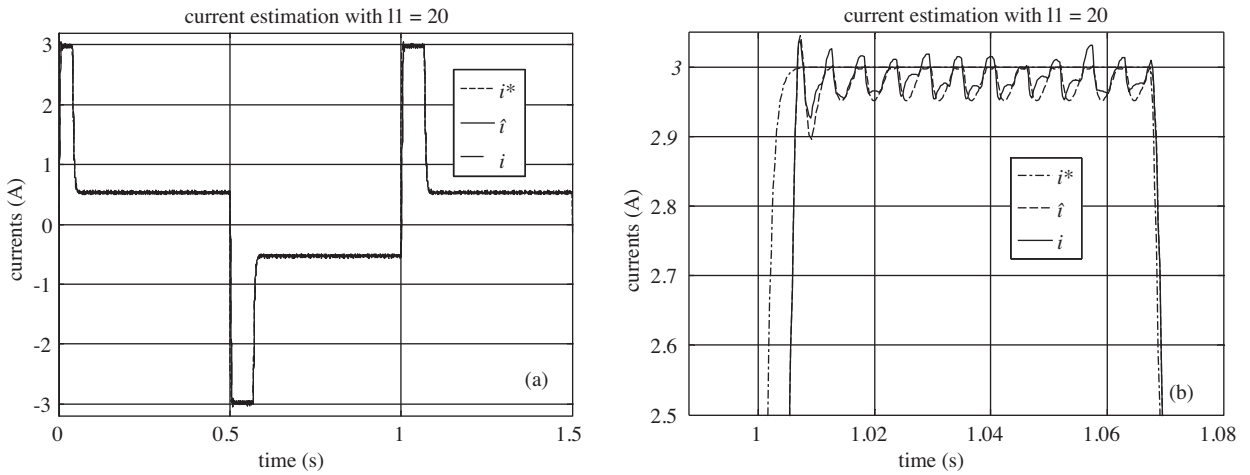

Figure 4. Simulated result for current estimation under closed loop speed control.

3.3. State-dependent gain method

In [7], it is proven by descriptive function analysis that chattering amplitude depends proportionally on the switching control gain M. Therefore, it would be helpful if a chattering suppression method could adapt the gain constant value M without losing the sliding mode condition [13]. In this method, M is reduced depending on the system state without spoiling the trajectory tracking convergence rate.

For implementation of the state-dependent gain adaptation, the sliding function is selected as given in (3) and the current control law with the feed-forward term u_{FF} can be described as follows:

$$u_2 = \underbrace{M(|s| + d_1)}_{M(e_i)} sign(s) + u_{FF} \tag{11}$$

where d_1 is a small constant and $M(e_i)$ is a new adopted control gain, which is expected to attenuate chattering. In adoptive gain $M(e_i)$, the term $M\,|s|$ reduces gain constant and the term Md_1 helps keep the trajectory tracking rate unchanged. Thus, the control version u_2 can be replaced with (4). The control inputs are generally bounded for all physical systems, therefore (11) may be modified by adding a limiter, which converts the system into 'the variable structure'.

$$u_2^* = \begin{cases} u_{\max} & \text{if} \quad u_2 \geq u_{\max} \\ M(|s| + d_1)sign(s) + k_e\omega & \text{if} \quad |\,u_2| < u_{\max} \\ -\,u_{\max} & \text{if} \quad u_2 \leq -u_{\max} \end{cases} \tag{12}$$

In our case, the actual control input u in (1) is bounded by DC link voltage $\mathrm{V}_{dc}\,(= u_{max})$. To analyse the closed loop system under control (11), the state error (the current tracking error) dynamics should be considered

and with the help of (1), it can be given in the following general form:

$$\frac{de_i}{dt} = f(i,t) - \frac{1}{L}u \tag{13}$$

where $f(i,t) = \dot{i}^* + (R/L)i + (k_e/L)\omega$ and $\dot{i}^*(= di^*/dt)$ denotes the derivative of the reference current, and u is the supply voltage corresponding to the control input, which will be replaced with u_2. Recall that the current tracking error was defined as the sliding surface $s = e = i^* - i$ in section 1.2. Inserting (11) into (13) results in

$$\dot{s} = f(i,t) - \frac{1}{L}M(|s| + d_1)sign(s) - u_{FF} \tag{14}$$

which verifies the stability of the closed control loop system if the following condition is fulfilled:

$$\left|L\dot{i}^* + Ri\right| < M\left(|s| + d_1\right) \tag{15}$$

3.4. Equivalent control-dependent gain method

Another gain adaptation method that may be used in system (13) is the equivalent control dependent gain adaptation. This can be achieved with the following control law:

$$u_3 = M(|\eta| + d_2)sign(s) + u_{FF} \tag{16}$$

where M and d_2 are positive constants and η is the average value of $sign(s)$, which can be obtained by using a first-order LPF. The equivalent control applied to the system input can be acquired by passing control u_3 through a 2nd first-order LPF. The aim of the first LPF is to scale down switching control gain $M(|\,\eta\,| + d_1)$ depending on the average value of $sign(s)$. The term $M|\,\eta\,|$ helps smooth the discontinuous control, and adding Md_1 preserves the trajectory convergence rate. The observer filter time constant $T_{c-equ}(= 1/f_{c-equ})$ should be selected as $T_{c-equ} << 1$.

The stability of the system under control u_3 (16) can be derived by inserting (16) into (13) instead of u, then the derivative of the sliding function s given in (3) results in

$$\begin{aligned} \frac{ds}{dt} &= f(i,t) - \frac{1}{L}M(|\eta| + d_2)sign(s) + \frac{1}{L}k_e\omega \\ &= L\dot{i}^* + Ri \; - M(|\eta| + d_2)sign(s) \end{aligned} \tag{17}$$

This finding implies the existence of the sliding mode $(s = 0)$. Trajectory tracking convergence of the motor current depends on the following condition remaining true:

$$|L\dot{i}^* + Ri| < M(|\eta| + d_2) \tag{18}$$

Note that the gain adaptation techniques used in controls u_2 and u_3 considerably reduce chattering. However, each control has different gain adaptation mechanisms; thus, the values of constants d_1 and d_2 can be different and they should be selected to keep the controllers' response time sufficiently short.

4. Simulations

To ensure the stability of the drive system under the gain adaptation-based control laws u_2 and u_3, the stability conditions (15) and (18) should be assessed. To test the stability and determine control gains, several simulations were performed by trial and error using the model constructed with Matlab/Simulink blocks shown in Figure 5. From this simulation, it was found that for $d_1 = d_2 = 0.9$, the stability condition (15) and (18) are properly satisfied. The simulation results are presented in Figure 6. In this figure the stability conditions (15) and (18) are represented by $x_2 < x_1$ and $x_2 < x_3$, respectively. Here, the variables are defined as follows: $x_1 = M(\,|s| + d_1)$, $x_2 = \left|L\dot{i}^* + Ri\right|$ and $x_3 = M(\,|\eta| + d_2)$.

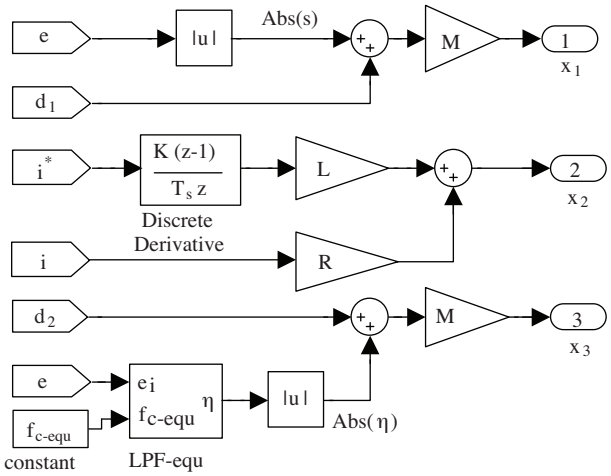

Figure 5. Simulink model used to test the stability conditions (15) and (19).

In the first simulation test, the speed control loop was excluded and a square-wave current reference was used for the inner current control with control version u_2. The obtained data are plotted in Figure 6(a). Enlargement of (a) is shown in (b), where a critical situation appears at the instant of 0.5 s during the simulation; however, the existence of condition $x_2 < x_1$ remains at the point of 0.5 s. The same test was repeated using a sine-wave current reference for both control versions u_2 and u_3. The data obtained with this test are plotted in Figure 6(c) and (e), respectively. The latter test was repeated with an activated speed control loop and again using a sine-wave speed reference with an amplitude of 200 rad/s. The data obtained in this final test are plotted in Figure 6 (d) and (f), respectively.

These last 2 results verify the stability conditions $x_2 < x_1$ and $x_2 < x_3$ remained under the speed controlled drives. It was noticed that increasing the design constant value d_1 delays the response time of control u_2, and the values $d_1 < 0.4$ and $d_2 < 0.25$ cannot satisfy the stability conditions for both controllers u_2 and u_3. Based on these findings, $d_1 = d_2 = 0.9$ was found satisfactory for experimental implementations.

5. Implementation and hardware set-up

5.1. Implementation issues

It is reported that in discrete-time computation of a control signal, the selection of the sampling rate is a critical design decision, and unfortunately, in continuous-time SMC, the desired closed loop bandwidth does not provide

any useful guidelines for the selection of the sampling rate [20]. Therefore, in computer-based motion control applications, the design and analysis are generally carried out in continuous-time due to the sample and hold process, but the control signals are computed in discrete-time. This is a usual assumption if the sampling rate is sufficiently fast.

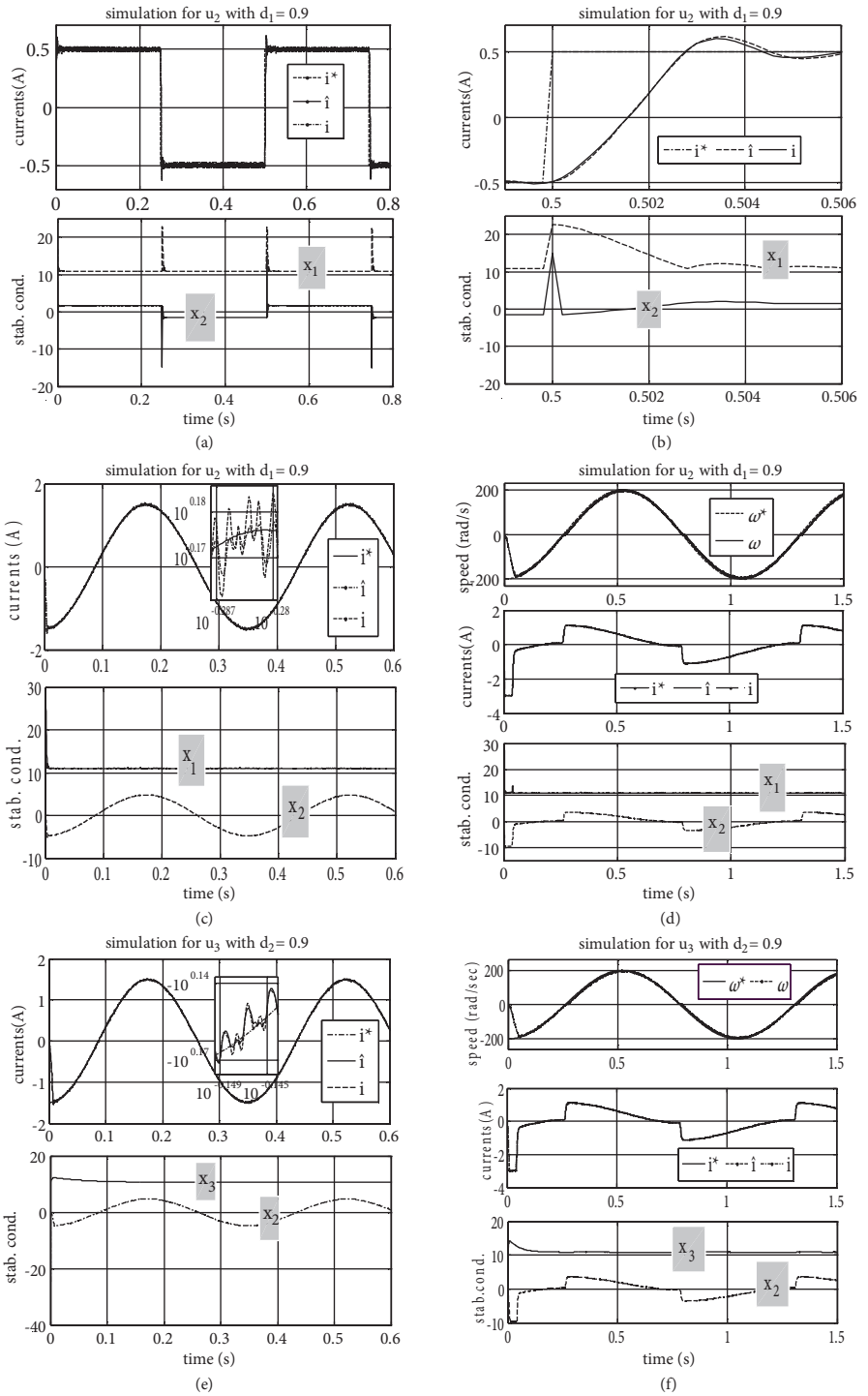

Figure 6. Simulated results of the stability conditions (15) and (19).

In this study, the controllers provide a continuous voltage command u_{av}, obtained by passing the discontinuous control signal through an LPF. This command is used to calculate the PWM switching times $T1$ and $T2$ for the H-bridge converter. Then, the armature average voltage u_0 during one switching period T_{sw} is

$$u_0 = \left(\frac{T1}{T_{sw}} - \frac{T2}{T_{sw}}\right) V_{dc} = (2D-1)V_{dc} \tag{19}$$

where D(= T1/T_{sw}) is the duty ratio and $T2$ =$T_{sw} - T1$. By varying the pulse width by changing D, the average voltage u_0 delivered to the motor changes and so does the current and speed of the motor. The model shown in Figure 7 calculates switching times $T1$ and $T2$, and then Xilinx FPGA generates PWM signals that activate the power converter IGBT transistors [28].

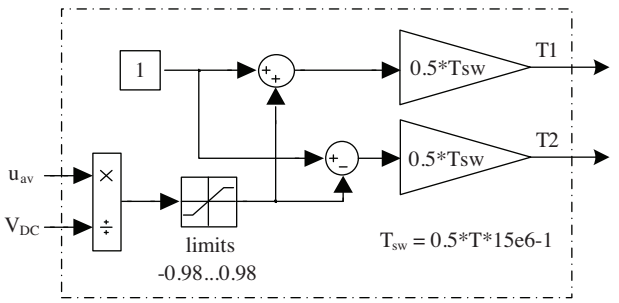

Figure 7. The model used to calculate PWM switching times.

The armature current is sensed by a hall-effect device fixed to the wire of the armature. The corresponding voltage signal of the measurement current is obtained by a resistor and the absolute value of that is sampled and used in the current loop control and/or observer structure.

The measured current might be influenced by the discontinuous nature of the PWM controlled H-bridge converter and hall-device depending on the switching frequency; therefore, a sliding mode current observer is introduced to construct a new sliding manifold which excludes the sensor and PWM dynamics. However, in conventional SMC, the filtered switching control signal does not improve the control system performance, and the chattering phenomenon incurred by high gain with the use of sign function remains [21]. But in our work, gain adaptation methods effectively scale down the switching gain to sufficient levels to eliminate chattering. The use of an LPF does not influence the discontinuous control performance due to fact that the reduced switching control gain in the proposed gain adaptation techniques reduces the time constant of the smoothing filter; therefore, the issue is not same as with an SMC which uses a high gain constant, which in turn influences control performance.

5.2. Hardware set-up

Experimental implementations were conducted using a hardware setup called the 'DC Experimental System', which includes a small-sized permanent magnet ESCAP DC motor driven though an H-bridge converter by a DSP-2 controller board. The hardware setup uses rapid control prototype (RCP) technologies, which can provide an easy transition from the model-based design to target implementation and eliminate the need for hand coding. A useful guide for the DSP-2 experimental system can be found in [28].

The DSP-2 is a controller board based on the TI TMS320C32-60 core and the FPGA Xilinx CS40-PQ240 which can communicate with PCs through a serial RS-232 cable or a USB port with a suitable serial RS-232 to

USB converter. The additional software toolbox 'DSP-2 Library' that runs under Matlab/Simulink eliminates the need for manual code generation, and offers its own rapid control prototype. The additional program 'DSP-2 Terminal' enables data visualization and parameter tuning during the operation intervals. The nominal parameters and rated data of the driven motor are listed in Table 1.

Table 1. Name plates and nominal motor parameters.

QUANTITY	Symbol	Unit
Nominal voltage	V_{dc}	12 V
No-load speed	ω	585 rad/s
Max. continuous current	I_a	1.5A
Max. continuous torque	T_{e-max}	28.4 mNm
Back-EMF constant	K_e	0.0195 V.s/rad
Torque constant	K_t	0.0195 N.m/A
Rotor resistance	R	2.5 Ω
Rotor inductance	L	0.3 mH
Inertia of otor	J	17.2e-7 kg.m2
Viscous damping constant	B	1e-6 N.m.s/rad

A block diagram depicting the overall structure of the drive system is given in Figure 8. The control algorithm was programmed with Matlab/Simulink blocks, which can be directly built in. Two different sampling times are used for the execution of the algorithm via the DSP-2 controller: a slower sampling-time of 200 μs and a faster one of 100 μs. As shown in Figure 8, a flywheel was mounted on the rotor shaft to cause the motor to receive a considerable amount of load current. In the experiment, 2 software switches sw_1 and sw_2 are employed to facilitate a practical transition between different tests.

The switch sw_1 is used to enable the speed controller to be switched on and off, and sw_2 is used to enable the selection of a current feedback signal (estimated or measured current). When the speed controller is excluded from the control loop by switch sw_1, the motor is driven by the current controller alone, using a command provided by the current reference generator. This operation mode is similar to direct torque-controlled drives. In this case, the motor is commanded by a square-wave current reference to facilitate capturing the transient response, which can be repeated continuously during motor operation. To regulate the rotor current, 3 different versions of control laws u_1, u_2 and u_3 given in (4), (12) and (17), respectively, were performed under different scenarios. All the control algorithms programmed using Simulink blocks are shown together in Figure 9. The design parameters for the controllers and observer are given in Table 2.

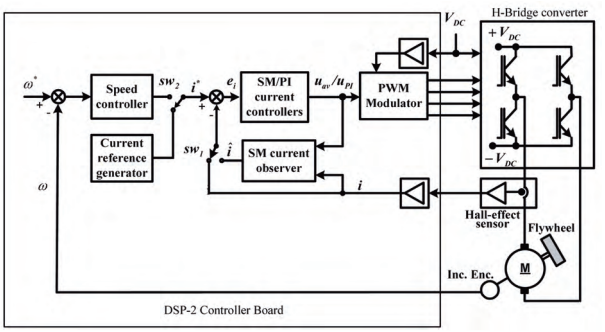

Figure 8. Structure of DC motor drive system used in experiments.

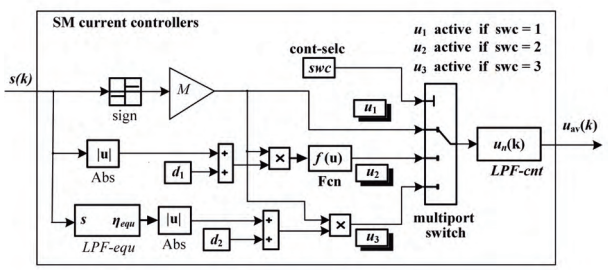

Figure 9. Structure of the SM current controllers u_1, u_2 and u_3.

Table 2. Controller design parameters.

PARAMETER	Symbol	Unit
Control gain constant for SMCs	M	12
Design constant foru_2	d_1	0.9
Design constant for u_3	d_2	0.9
Cut-off frequency of LPF-cnt	f_{c-cnt}	250 Hz
Cut-off frequency of LPF-equ	f_{c-equ}	20 Hz
Cut-off frequency of LPF-obs	f_{c-obs}	20 Hz
Observer gain constant	l_1	20

5.3. Experiments

The main goal is to show the effectiveness of the chattering reduction methods through real-time experimentation. To this end, this study examined some of the well-known methods in combination with the proposed methods on a current-controlled DC drive system, in which current control strategy is very similar to the torque control (considering the relation $t_e^* = k_t i^*$) needed with minimized ripple in many applications. Consequently, the speed control loop is omitted for the first 3 tests of the experiment. However, in the third test, 3 versions of the proposed current controller were examined to reveal whether their performance is preserved when the speed loop control is activated. The following hardware experiments were performed:

Test 1: 2 different cases were tested:

a) The control versions u_1, u_2 and u_3 were separately executed using a smoothing filter and a lowered sampling rate of 1/200 μs. The measured current i was used in the feedback loop to determine how well each control law reduces chattering alone without using the observer-based method.

b) The test was repeated to examine how the observer-based method attenuates chattering alone. For this purpose the auxiliary observer loop was activated by the handling switch sw_1, which replaces the measured current i with the estimated current $\hat{i}$. The results obtained in Test 1(a) and Test 1(b) are comparatively presented in the 1st and 2nd column of Figure 10, respectively. The figures in the 1st column of Figure 10 show that performing each of the gain adaptation methods alone in control versions u_2 and u_3 is fairly good at reducing chattering compared to conventional version u_1, However, the chattering amplitude is considerably attenuated with the use of the observer-based method, as shown in the 2nd column of Figure 10.

Test 2: To determine how an increased sampling rate reduces discretization chattering, Test 1(a) was repeated with an increased sampling rate of 1/100 μs. The resulting data were plotted in Figure 11, which verifies that increasing the sampling rate attenuates chattering considerably for all the control versions. Unlike the observer-based method, however, u_2 was found to be the most efficient control version for chattering suppression, as shown in Figure 11 (b).

Test 3: To achieve chattering suppression more efficiently, combinations of each control version u_1, u_2 and u_3 with the observer-based method were used with a smoothing filter and an increased sampling rate. The observer-based method was performed as in Test 1(b), with the use of an increased sampling rate of 1/100 μs. The recorded data were plotted in Figure 12, which verifies that the proposed method reduces chattering amplitude more efficiently and has virtually the same effects on all the control versions even though the same gain constant value ($M = 12$) was used. It is should be noted that the amplitude of the discontinuous control signal generated by control versions u_2 and u_3 was found to be lower than that of the control version u_1. This can be clearly seen by comparing (b) and (c) with (a) in Figure 12. This finding verifies that the gain

adaptation methods used in the controls (11) and (16) perform efficiently to reduce the amplitude of the gain constant as well as to attenuate chattering. Comparing the enlargements in Figure 12(a), (b), and (c) shows that the control version u_2 exhibits the fastest and least disturbed response.

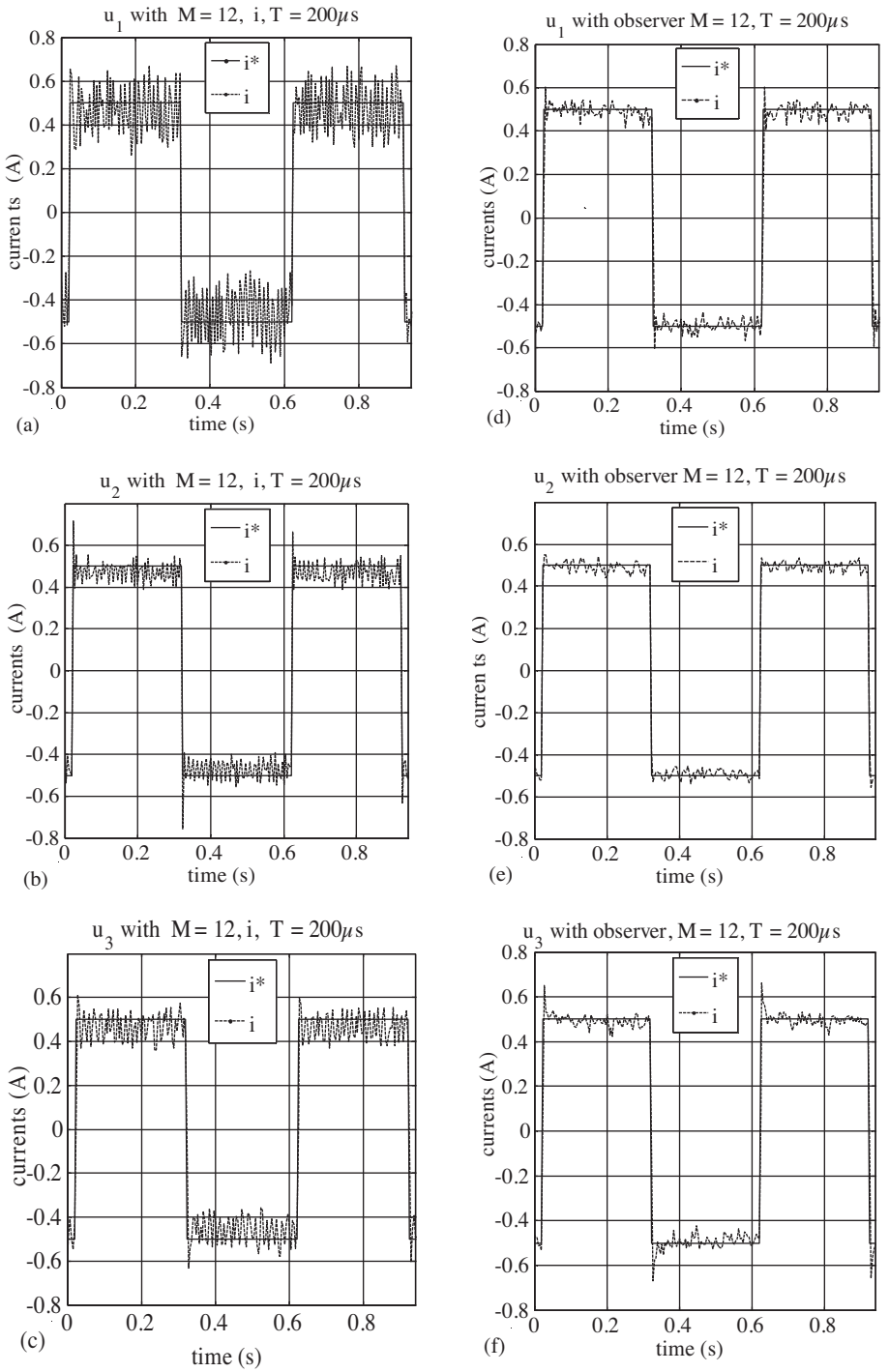

Figure 10. The recorded results of Test 1(a) (in the first column) and Test 1(b) (in the second column). In both columns, the traces show the current trajectory response provided by control laws u_1, u_2 and u_3, respectively.

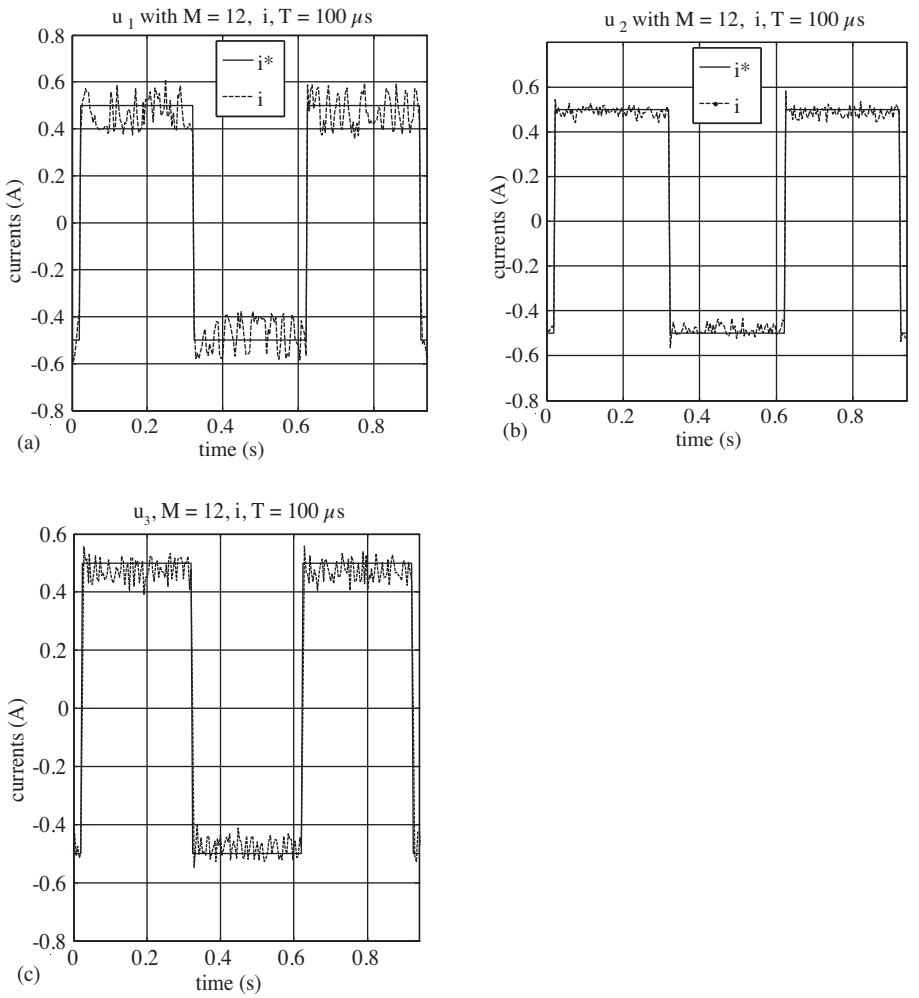

Figure 11. Test2 results obtained using increased sampling rate $1/100\,\mu$sec. Traces in (a), (b), (c) were obtained for control laws u_1, u_2, and u_3 respectively.

Test 4: The proposed method assessed in Test 3 was examined again when the speed control loop was activated via sw_2. In this case, the current reference generator was removed from the loop and a current reference was provided by a speed controller, so a limiter was required to ensure that the motor operated in current control mode when the armature current exceeded its rated value during transient or overloading conditions. Furthermore, performance comparisons between the proposed SM controllers and the conventional PI current controller were made under a very light load condition supplied by a flywheel mounted on the rotor shaft. The data obtained in this comparative test are plotted in Figure 13.

The traces in Figure 13(a) and (b) show the speed and current tracking for the control versions u_1 and u_2. In these figures, the current data were multiplied by 30 for illustrative purposes, and the figures next to (a) and (b) show an enlargement of the current signals with actual magnitude. For both the PI-based current control and SMC version u_3, the speed tracking figures are omitted and only current tracking is shown in (c) and (d). Comparing these experimental results verifies that the proposed SM current controller provides faster response and lower current ripple than the conventional PI-based current controller, and as the control u_3 was found to be more efficient at chattering reduction in cases when the speed control loop was closed. Moreover, it

was observed that the current ripple can be reduced if the current reference at the output of the speed controller is filtered for PI-based current control, but this filtering has an adverse effect on SM-based current controls.

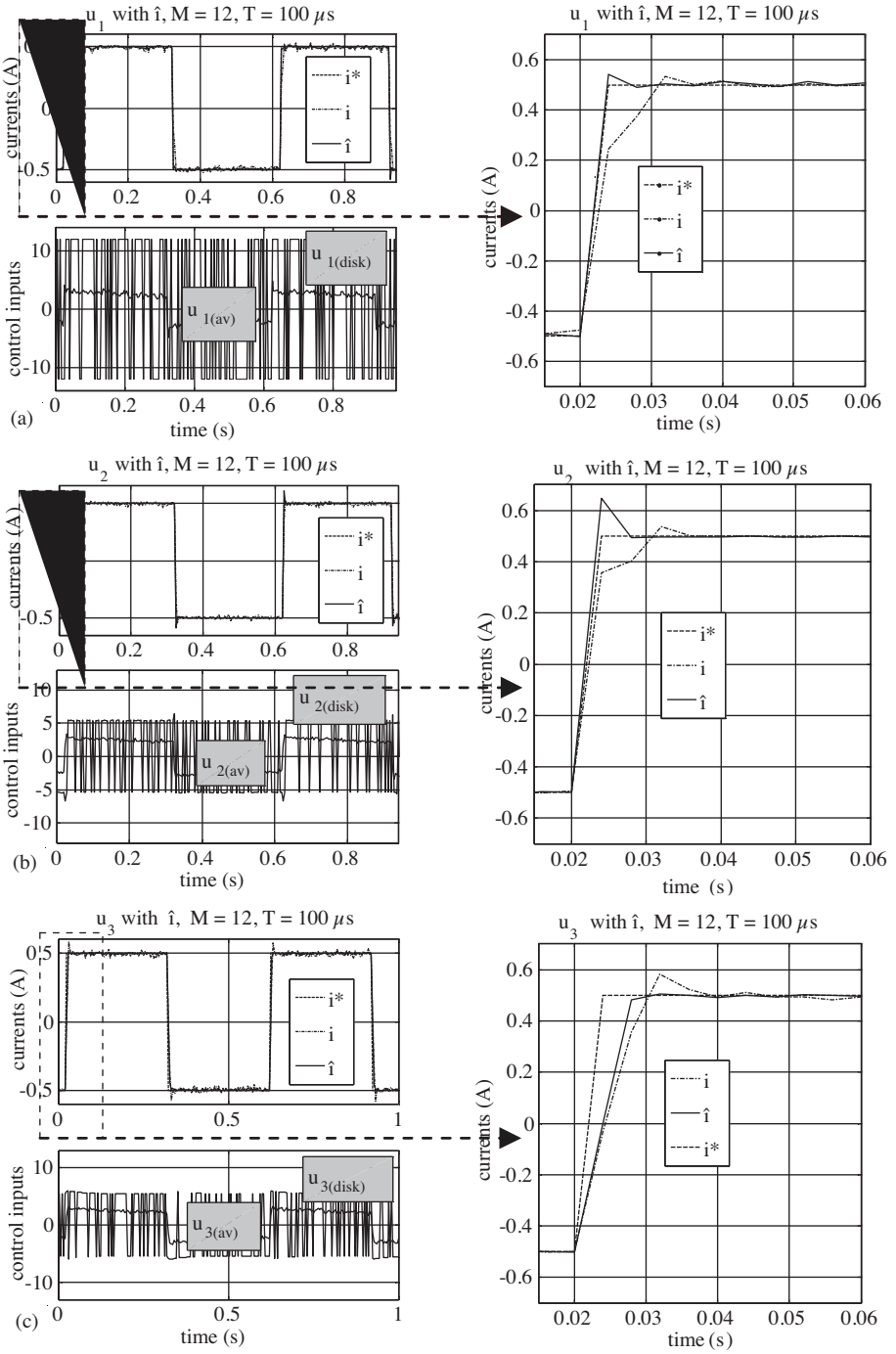

Figure 12. Test 4 results. In first column, upper traces show currents $i^*, \hat{i}$ and i for controls u_1, u_2 and u_3, respectively, and bottom traces show corresponding discontinuous control input and its average value. Enlargements of each current tracking and convergence of current estimate are shown in the second column with actual magnitude.

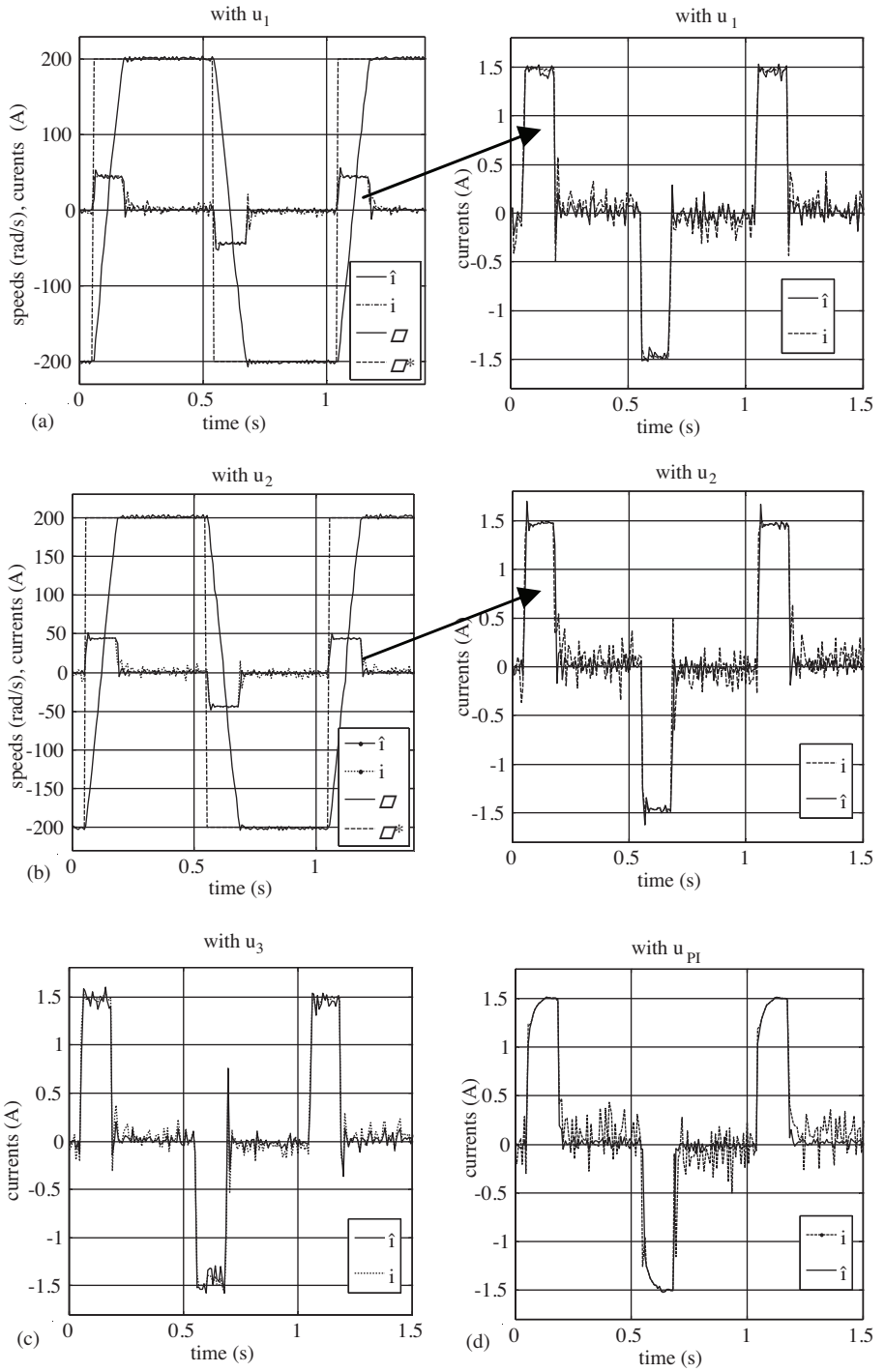

Figure 13. Test 4 results when speed loop was closed and measured current feedback was used with speed and current response to square-wave speed trajectory.

6. Conclusion

Several chattering suppression methods for current regulation of DC motor drives were examined experimentally. It has been concluded that chattering elimination is not a trivial problem for digital implementation of SMC, and that discretization chatter may be indistinguishable from the chattering caused by system unmodeled dynamics.

Using switching gain adaptations based on state-dependent or equivalent-control-dependent approaches, SMC was enabled to apply to such systems that should be controlled by "on/off" switching, which is the only admissible operation mode for electric drives through power electronics converters. However, it was experimentally demonstrated that while these 2 methods considerably attenuate chattering, they do not eliminate it fully. Thus, a new combination of gain adaptation and the state-observer method with the use of an increased sampling rate and a smoothing filter was found to be the best way to suppress chattering. This proposed method may increase the complexity of the control structure, but offers the advantages of SMC methodology – robustness and fast dynamic response. This was determined by experimental comparison between the SMC-based schemes and a conventional PI-based scheme. Further work will focus on an integrated (single-loop) sensorless speed control of PM DC drives using SMC with gain adaptation methods.

References

[1] V.I. Utkin, "Variable structure systems with sliding modes", *IEEE Trans. Autom. Control*, Vol. 22, pp. 212-222, 1977.

[2] J.Y. Hung, W.B. Gao, J.C. Hung, "Variable structure control: A survey", *IEEE Trans. Ind. Electron.*, Vol. 40, pp. 2-22, 1993.

[3] V.I. Utkin, "Sliding mode control design principles and applications to electric drives", *IEEE Trans. Ind. Electron.*, Vol. 40, pp. 23-36, 1993.

[4] V.I. Utkin, J. Guldner, J. Shi, "Sliding mode control in electromechanical systems", New York: Taylor & Francis, 1999.

[5] T.L. Chern, J.S. Wong, "DSP based integral variable structure control for DC motor servo drives", *IEE Proceedings – Control Theory & Applications*, Vol. 142, pp. 444-450, 1995.

[6] Z. Yan, C. Jin, V.I. Utkin, "Sensorless sliding-mode control of induction motors", *IEEE Trans. Ind. Electron.*, Vol. 47, pp. 1286–1297, 2000.

[7] A. Sabanovic, K. Jezernik, N. Sabanovic, "Sliding modes applications in power electronics and electrical drives", in *Variable Structure Systems: Towards the 21st Century*, Vol. 274, X. Yu and J.-X. Xu, Eds., Berlin, Springer-Verlag, pp. 223-251, 2002.

[8] K. Abidi, A. Sabanovic, "Sliding-mode control for high-precision motion of a piezostage", *IEEE Trans. Ind. Electron.*, Vol. 54, pp. 629-637, 2007.

[9] C. Rossi, A. Tonielli, "Robust control of permanent magnet motors: VSS techniques lead to simple hardware implementations", *IEEE Trans. Ind. Appl.*, Vol. 41, pp. 451-460, 1994.

[10] S. Tokat, "Sliding mode controlled bioreactor using a time-varying sliding surface", *Transactions of the Institute of Measure and Control,* Vol. 31, pp. 435-456, 2009.

[11] S. Labiod, "A neuro-fuzzy-sliding mode controller using nonlinear sliding surface applied to the coupled tanks system", *International Journal of Automation and Computing*, Vol. 6, pp.72-80, 2009.

[12] H.K. Halil, "Nonlinear System," New Jersey: Pearson Educ. Inc., 2000.

[13] H. Lee, V.I. Utkin, "Chattering suppression methods in sliding mode control systems", *Annual Reviews in Control*, Vol. 31, pp. 179-188, 2007.

[14] V.I. Utkin, H. Lee "The chattering analysis", *Proc. of 12th International Power Electronics and Motion Control Conference on Ind.* EPE_PEMC, Portoroz, Slovenia 2006.

[15] A.G. Bondarev, S.A. Bondarev, N.E. Kostyleva, and V.I. Utkin, "Sliding modes in systems with asymptotic state observers", *Autom. Remote Control*, Vol. 46, pp. 679-684, 1985.

[16] J.J. Slotine, W. Li, Applied Nonlinear Control, Prentice Hall, 1991.

[17] M. Ertugrul, O. Kaynak, A. Sabanovic, K. Ohnishi "A generalized approach for Lyapunov design of sliding mode controllers for motion control applications", *Proc. 4th Int'l. Workshop on Advanced Motion Control*, Vol. 1, pp. 407-412, 1996.

[18] A. Levant, "Higher-order sliding modes, differentiation and output feedback control", *International Journal of Control*, Vol. 76, pp. 924-941, 2003.

[19] A. Pisano, A. Davila, L. Fridman, E. Usai, "Cascade control of PM-DC drives via second-order sliding-mode technique", *IEEE Trans. Ind. Electron*, Vol. 55, pp. 3347-3853, 2008.

[20] K.D. Young, V.I. Utkin, U. Ozguner, "A control engineer's guide to sliding mode control", *IEEE Trans. Control Syst. Technol.*, Vol. 7, pp. 328-342, 1999.

[21] J.X. Xu, Y.J. Pan, T.H. Lee, "Sliding mode control with closed-loop filtering architecture for a class of nonlinear systems", *IEEE Trans. Circuits and Sys.*: Express Briefs, Vol. 51, pp. 168-173, 2004.

[22] M. Dal, R. Teodorescu. "Chattering suppression for DSP based sliding mode current control of PM DC drives" *Proc. 35th Annual Conference of the IEEE Ind. Elo. Society*, pp. 1476-1481, 2009.

[23] W. Leonhard, Control of Electric Drives, London, Springer-Verlag, 1985.

[24] Y.H. Chang, H.W. Lin, G. Chen, "Compensation on Hall effect sensor of PWM switching control", Journal of Magnetism and Magnetic Materials, Vol. 282, pp. 307-310, 2004.

[25] P. Vas, Vector Control of Ac Machines, Oxford, Clarendon, 1990.

[26] **"**DSP based sensorless PM DC drives using a proportional plus sliding mode control" *The 2nd IFAC International Conference on Intelligent Control Systems and Signal Processing* ICONS'09, 21-23, Sept. 2009, Istanbul, Turkey

[27] S. Drakunov, "On adaptive quasioptimal filter with discontinues parameters", *Automation and Remote Control*, Vol. 44, pp. 1167-1175, 1983.

[28] User manual for programming DSP-2, "DC experimental system", Maribor University, Slovenia, 2004.